IOP Conference Series: Materials Science and Engineering

OPEN ACCESS

Melt solidification in the ceramic system CaO-Al_2O_3-SiO_2

To cite this article: V I Lutsyk *et al* 2011 *IOP Conf. Ser.: Mater. Sci. Eng.* **18** 112005

View the article online for updates and enhancements.

You may also like

- Propagation direction of geodesic acoustic modes driven by drift wave turbulence
M. Sasaki, K. Itoh, T. Kobayashi et al.
- Effects of energetic particle phase space modifications by instabilities on integrated modeling
M. Podestà, M. Gorelenkova, E.D. Fredrickson et al.
- Crystallization paths in SiO_2-Al_2O_3-CaO system as a genotype of silicate materials
V I Lutsyk and A E Zelenaya

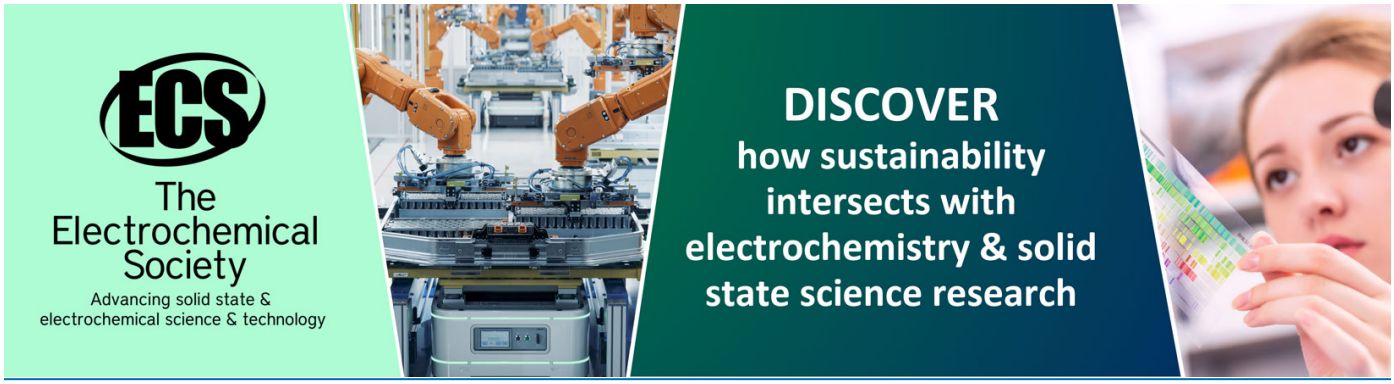

This content was downloaded from IP address 3.17.25.60 on 27/04/2024 at 20:29

IOP Conf. Series: Materials Science and Engineering **18** (2011) 112005 doi:10.1088/1757-899X/18/11/112005

Melt solidification in the ceramic system $CaO-Al_2O_3-SiO_2$

V I Lutsyk, A E Zelenaya, V V Savinov

Physical Problems Department, Buryat Scientific Center of RAS (Siberian Branch), 8 Sakhyanova st., Ulan-Ude, 670047, Russian Federation

E-mail: vluts@pres.bscnet.ru

Abstract. Technique of T-x-y diagram for system $CaO-Al_2O_3-SiO_2$ computer simulation by the use of kinematical surfaces has been suggested. Original 245 crystallization paths were found.

1. Introduction

The system $CaO-Al_2O_3-SiO_2$ (C-A-S) has a great practical importance [1-2]. Its T-x-y diagram models [3-5] solve series of applied tasks, but don't allow to present full topological structure of diagram for the obtaining of concentration fields with the unique crystallization schemes. In particular, the immiscibility surfaces and 4 liquidus surfaces (C_3S, C_3S_2, C_3A, CA_6) are absent in Vladimir Danek's model [3, P. 147]: "The immiscibility region near the SiO_2 apex was neglected in the calculation as such behavior is not considered in the thermodynamic model. Furthermore, because of the lack of thermodynamic data, the crystallization of rankinite, tricalcium silicate, tricalcium aluminate, and calcium hexaaluminate was not included in the calculation". In the model, considered in [4], there isn't one binary eutectic in system C-A. As a result, a liquidus surface of $C_{12}A_7$ is internal and, unlike the experimental data [5], doesn't adjacent to the binary system. The model calculated by the thermodynamics software CaTCalc [6] doesn't include three liquidus surfaces (C_3S, C_3S_2, $C_{12}A_7$).

The kinematical method is used for T-x-y diagram simulation [7], when a kinematical surface is produced by the motion of forming line along to the directing ones described by the interpolating polynomials. Approximating possibilities of the kinematical simulation were checked by the investigation of saddle surface (as the most complex boundary of phase regions) described by the Sheffe's model [8-9]. When kinematical saddle surface was simulated by 7 points (3 simplex vertexes, 3 points on its sides and 1 – within the simplex), a standard deviation with the Sheffe's saddle (in 66 sites of concentration triangle with the step 0,1) was about 2,5 degrees and the most discordance (5-8 degrees) was observed in 17 points. The saddle points differ in the concentration coordinates: polynomial model (0,181; 0.384; 0,435) and kinematical one (0,159; 0.394; 0,447). When the kinematical surface was taken with 3 internal directing curves and simulated by 21 point (3 tops, 3 triads on the simplex' edges and 3 internal triads), the disagreements in temperatures were lowered and the concentration coordinates of saddle points for both models essentially approach each other: 0,194; 0.391; 0,415 – for a kinematical model.

2. Computer model of system $CaO-Al_2O_3-SiO_2$

The coordinates of 14 binary points (9 eutectics (e) and 5 peritectics (p)), 16 ternary points (6 eutectics (E), 9 quasiperitectics (Q) and the point of four-phase mass regrouping with two allotropies of SiO_2 (U)), 10 binary (R_1-R_{10}) and 2 ternary compounds (R_{11} and R_{12}) are taken for the computer model

© 2011 Ceramic Society of Japan.

Published under licence by IOP Publishing Ltd

construction [1, 7]. Also the coordinates of inflections on monovariant liquidus curves should be taken into account. The following designation of compounds are used: R_1 – C_3S, R_2 – C_2S, R_3 –C_3S_2, R_4 – CS, R_5 – A_3S_2, R_6 – C_3A, R_7 – $C_{12}A_7$, R_8 – CA, R_9 – CA_2, R_{10} – CA_6, R_{11} – C_2AS, R_{12} – CAS_2, where R_1, R_3, R_6, R_{10} are ingongruently melting compounds and R_2, R_4, R_5, R_7, R_8, R_9, R_{11}, R_{12} are the congruently melting ones.

The phase diagram involves 16 unruled surfaces (15 liquidus surfaces S and one immiscibility surface i) (table 1, figure 1a), 80 ruled surfaces ($77S^r+3i^r$), 16 horizontal complexes at the invariant points temperatures (H) and 16 vertical planes of triangulation (figure 1b).

Unruled surfaces with more then four points on their contour are constructed by the fragmentation into the more simple parts. In such way the surfaces S_2, S_4, S_6, S_7, S_{11}, S_{14}, S_{16} are given by two parts, and the surfaces S_9, S_{12}, S_{13}, S_{15} – by three parts. E.g., surface S_{15} has seven points on contour, the horizontal curve p_3U and the cut mkn remained after intersection with immiscibility surface (figure 2). It includes 3 fragments np_3U, $mknUe_4$ and SiO_2me_4, simulated by a common directing curve $p_3(n,U)(m,e_4)SiO_2$ and by 2 forming lines $n(n,U)U$ and $m(m,e_4)e_4$. The parts of common directing line are used for the construction of different surface's fragments. So line's parts $p_3(n,U)$, $(n,U)(m,e_4)$ and $(m,e_4)SiO_2$ form the fragments snp_3U, $mknUe_4$ and SiO_2me_4 accordingly. The cut is given as directing line $n(n,k)k(m,k)m$ with five points on the intermediate surface's fragment. The intermediate point (p_3,U) should be assigned at temperature $T_{U(p3)}$ for the horizontal line p_3U generation.

Table 1. Contours of unruled surfaces (figure 1a).

Name	Contour	Name	Contour
i	k^0nkm	$S_8(C_3S)$	$p_1Q_1Q_2e_1$
$S_1(C)$	$CaOp_1Q_1p_4$	$S_9(C_2S)$	$e_1Q_2Q_3E_1Q_4(Q_4,Q_9)Q_9p_2R_2$
$S_2(C_3A)$	$p_4Q_1Q_2Q_3e_6$	$S_{10}(C_3S_2)$	$p_2Q_9E_2e_2$
$S_3(C_{12}A_7)$	$e_6Q_3E_1e_7R_7$	$S_{11}(CS)$	$e_2E_2(E_2,E_3)E_3(E_3,E_4)E_4e_3R_4$
$S_4(CA)$	$e_7E_1Q_4Q_5e_8R_8$	$S_{12}(C_2AS)$	$Q_4Q_5(Q_5,Q_6)Q_6E_6E_3(E_2,E_3)E_2Q_9$
$S_5(CA_2)$	$e_8Q_5(Q_5,Q_6)Q_6e_9$	$S_{13}(CAS_2)$	$E_3(E_3,E_4)E_4(E_4,E_5)E_5Q_8(Q_7,Q_8)Q_7E_6$
$S_6(CA_6)$	$e_9Q_6E_6Q_7p_5$	$S_{14}(S^t)$	$e_3E_4(E_4,E_5)E_5Up_3$
$S_7(A)$	$Al_2O_3p_5Q_7(Q_7,Q_8)Q_8e_5$	$S_{15}(S^c)$	$SiO_2mknp_3Ue_4$
		$S_{16}(A_3S_2)$	$e_4UE_5Q_8e_5R_5$

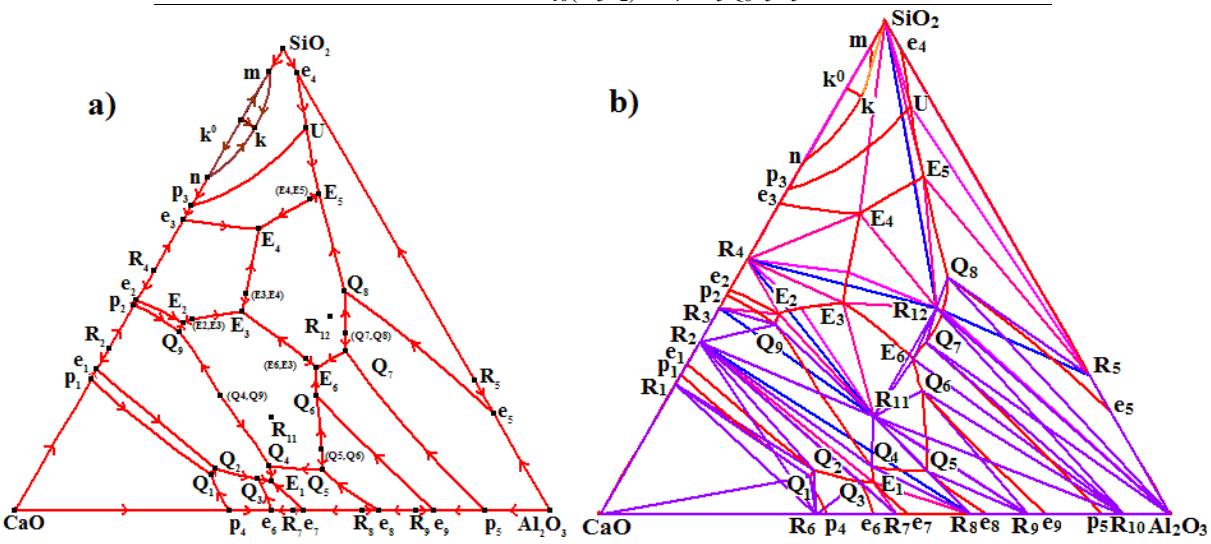

Figure 1. XY projections of liquidus surfaces and immiscibility cupola (a), all diagram surfaces (b).

16 invariant transformations characterize the considered system. There are nine quasiperitectic transformations (Q), six eutectic ones (E) and one transformation of the mass regrouping with two allotropies of SiO_2 (U): $L(Q_8)+Al_2O_3\rightarrow R_5+R_{12}$, $L(Q_5)+R_9\rightarrow R_8+R_{11}$, $L(Q_7)+Al_2O_3\rightarrow R_{10}+R_{12}$, $L(Q_6)+R_9\rightarrow R_{10}+R_{11}$, $L(Q_1)+CaO\rightarrow R_1+R_6$, $U+SiO^{tr}_2\rightarrow R_5+SiO^{cr}_2$, $L(Q_2)+R_1\rightarrow R_2+R_6$,

$L(E_6)\rightarrow R_{10}+R_{11}+R_{12}$, $L(Q_4)+R_{11}\rightarrow R_2+R_8$, $L(Q_3)+R_6\rightarrow R_2+R_7$, $L(E_5)\rightarrow R_5+R_{12}+SiO_2$, $L(E_1)\rightarrow R_2+R_7+R_8$, $L(Q_9)+R_2\rightarrow R_3+R_{11}$, $L(E_2)\rightarrow R_3+R_4+R_{11}$, $L(E_3)\rightarrow R_4+R_{11}+R_{12}$, $L(E_4)\rightarrow R_4+R_{12}+SiO_2$.

Phase diagram includes one one-phase region (L), 33 two-phase regions (L_1+L_2, L+CaO, $L+R_1$, $L+R_2$, $L+R_3$, $L+R_4$, $L+R_5$, $L+R_6$, $L+R_7$, $L+R_8$, $L+R_9$, $L+R_{10}$, $L+R_{11}$, $L+R_{12}$, $L+SiO^{cr}_2$, $L+SiO^{tr}_2$, $L+Al_2O_3$, R_1+R_6, R_2+R_6, R_2+R_7, R_2+R_8, R_2+R_{11}, R_3+R_{11}, R_4+R_{11}, R_5+R_{12}, R_8+R_{11}, R_9+R_{11}, $R_{10}+R_{11}$, $R_{10}+R_{12}$, $R_{11}+R_{12}$, R_4+R_{12}, $R_{12}+SiO_2$, $R_{12}+Al_2O_3$) and 46 three-phase regions ($L_1+L_2+SiO_2$, $L+CaO+R_1$, $L+CaO+R_6$, $L+R_1+R_2$, $L+R_1+R_6$, $L+R_2+R_3$, $L+R_2+R_6$, $L+R_2+R_7$, $L+R_2+R_8$, $L+R_2+R_{11}$, $L+R_3+R_4$, $L+R_3+R_{11}$, $L+R_4+R_{11}$, $L+R_4+R_{12}$, $L+R_4+SiO^{cr}_2$, $L+R_5+R_{12}$, $L+R_5+SiO^{u}_2$, $L+R_5+SiO^{d}_2$, $L+R_5+Al_2O_3$, $L+R_6+R_7$, $L+R_7+R_8$, $L+R_8+R_9$, $L+R_8+R_{11}$, $L+R_9+R_{10}$, $L+R_9+R_{11}$, $L+R_{10}+R_{11}$, $L+R_{10}+R_{12}$, $L+R_{11}+R_{12}$, $L+R_{10}+Al_2O_3$, $L+R_{12}+Al_2O_3$, $L+R_{12}+SiO_2$, $CaO+R_1+R_6$, $R_1+R_2+R_6$, $R_2+R_3+R_{11}$, $R_2+R_6+R_7$, $R_2+R_7+R_8$, $R_2+R_8+R_{11}$, $R_3+R_4+R_{11}$, $R_4+R_{11}+R_{12}$, $R_4+R_{12}+SiO_2$, $R_5+R_{12}+SiO_2$, $R_5+R_{12}+Al_2O_3$, $R_8+R_9+R_{11}$, $R_9+R_{10}+R_{11}$, $R_{10}+R_{11}+R_{12}$, $R_{10}+R_{12}+Al_2O_3$).

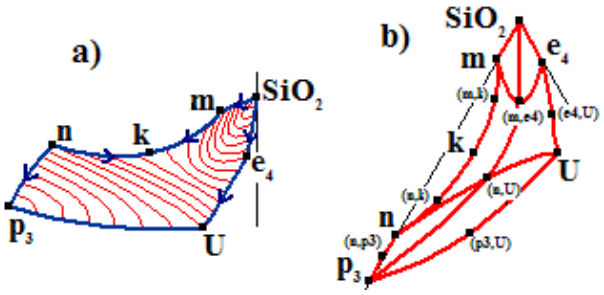

Figure 2. Space model (a) and fragmentation (b) of surface S_{15}.

3. Crystallization paths

No more then 10 crystallization paths have been usually analyzed in the traditional tutorials for the system $CaO-Al_2O_3-SiO_2$ [2]. Computer model gives possible to consider the crystallization paths for all diagram concentration fields, 117 of which are two-dimensional, 163 - one-dimensional and 45 - zero-dimensional(figure 1b). Let' consider the compositions given in the CaO crystallization region.

So the melt G_1(0.722; 0.162; 0.116), arranged in the triangle R_1R_6CaO (figure 5a-b), moves along the ray $CaO-G_1$ (on the concentration projection) to the liquidus line p_1Q_1 while the passing through two-phase region L+CaO. Then it falls into three-phase region L+CaO+R1 and shifts along the line of monovariant equilibrium p_1Q_1. A reaction $L(Q_2)+R_1\rightarrow R_2+R_6$ is finished with the deficit of melt on horizontal complex $R_1Q_1R_6CaO$ at temperature Q_1 and beneath there are only crystals CaO, R_1 and R_6.

The melt G_2(0.638; 0.105; 0.257), given in triangle $R_1R_2R_6$ (figure c-d), moves along CaO-G to liquidus line p_1Q_1 at the going through two-phase region L+CaO. Next motion along monovariant equilibrium line p_1Q_1 to point Q_1 corresponds the three-phase region L+CaO+R1. Later the melt puts into three-phase region L+R1+R6 and its crystallization path coincides with the curve Q_1Q_2 to point Q_2. The reaction $L(Q_2)+R_1\rightarrow R_2+R_6$ is compelled with the melt deficit on the horizontal complex $R_1R_2Q_1R_6$ at the temperature Q_2. Below this complex there are crystals R_1, R_2 and R_6.

Composition G_3(0.706; 0.248; 0.046) also is given in subsystem $R_1R_2R_6$ but other concentration field (figure 5e). The melt G_3 shifts along segment $CaO-G_2$ to monovariant line p_1Q_1 within the region L+CaO and along the fragment of line p_1Q_1 within the region L+CaO+R1. Then the melt appears in region L+R1 and its crystallization paths across the liquidus surface $R1(p_1e_1Q_2Q_1)$ to line e_1Q_2. The motion along line e_1Q_2 to point Q_2 corresponds the region L+R1+R2. The reaction $L(Q_2)+R_1\rightarrow R_2+R_6$ ends with the melt deficit on the plane $R_1R_2Q_2R_6$ and beneath there are only crystals R_1, R_2 and R_6.

The melt G_4(0.604; 0.017; 0.379), situated in triangle $R_2R_6R_7$ (figure 3f), moves along segment $CaO-G_1$ to point (1) on the liquidus line p_4Q_1 at the passing through two-phase region L+CaO (figure 3g). Next it falls into three-phase region L+CaO+R6 and shifts along line p_4Q_1 to point (2). Then melt moves the liquidus surface $p_4Q_1Q_2Q_3$ to point (3) on line Q_2Q_3 within region L+R6 and moves along

line Q_2Q_3 to point Q_3 at the going through L+R2+R6. The reaction $L(Q_3)+R_6 \rightarrow R_2+R_7$ is finished on horizontal complex $R_6R_2Q_3R_7$ and below there are only R_2, R_6 and R_7.

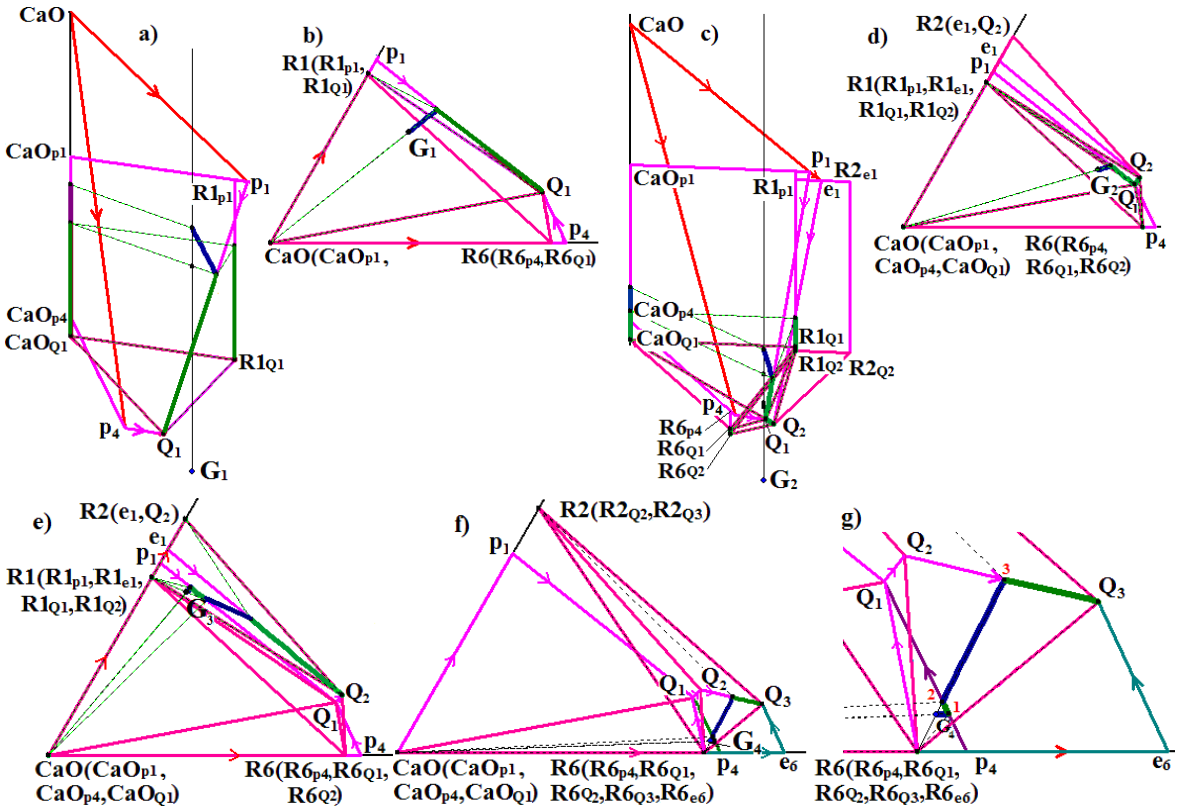

Figure 3. TXY models (a, c) and XY projections of melts trajectories G_1 (b), G_2 (d), G_3 (e) and G_4 (f, g is enlarged fragment).

4. Conclusions

Obtained $CaO\text{-}Al_2O_3\text{-}SiO_2$ model can be used as a template for the simulation of different silicate systems computer models (such as a system $MgO\text{-}Al_2O_3\text{-}SiO_2$ with similar but more simple topological structure). The crystallization stage for given composition also can be considered on the material balance diagrams. The elaborated phase diagrams computer models make possible to calculate the crystallization paths and microstructures formation at the silicate materials design.

References

[1] Toropov N A, Bazarkovsky V P, Lapshin V V et al. 1972 *Diagram of Silicate System. Ternary Silicate Systems* vol 3 (Leningrad: Nauka) pp 184-190 (In Russian)
[2] Patshenko A A, Aleksenko N V et al. 1977 *Phisical Chemistry of Silicate* ed A A Patshenko (Kiev: Vyshcha schkola) (In Russian)
[3] Danek V 2006 *Physico-chemical Analysis of Molten Electrolytes* (New York: Elsevier)
[4] Berman R G and Brown T H 1984 *Geochim. et Cosmochim. Acta* **48** 661
[5] Levin E M, Robbins C R and McMurdie H F 1964 *Phase Diagrams for Ceramists* (Ohio: American. Ceramic Society)
[6] Shobu K 2009 *CALPHAD* **33** 279
[7] Lutsyk V I, Zyryanov A M and Zelenaya A E 2008 *Russ. J. Inorg. Chem* **53** 792
[8] Scheffe H 1957 *J. Royal Statistical Soc* **20** 344
[9] Lutsyk V I 1987 *Analysis of Liquidus Surfaces in Ternary Systems* (Moscow: Nauka Publ. House) (In Russian)